Journal of Power Sources 267 (2014) 380–387

Contents lists available at ScienceDirect

Journal of Power Sources

journal homepage: www.elsevier.com/locate/jpowsour

Synthesis of PtCu nanowires in nonaqueous solvent with enhanced activity and stability for oxygen reduction reaction

Bing Chen [a], Daojian Cheng [a, *], Jiqin Zhu [b, *]

[a] State Key Laboratory of Organic–Inorganic Composites, Beijing University of Chemical Technology, Beijing 100029, China
[b] State Key Laboratory of Chemical Resource Engineering, Beijing University of Chemical Technology, 100029 Beijing, China

HIGHLIGHTS

- Cu@CuPt core@shell nanowires were synthesized in organic solvent medium.
- PtCu nanowires exhibit superior catalytic activity toward the oxygen reduction reaction.
- PtCu nanowires show much better durability than the commercial Pt/C catalyst.
- Theoretical studies are used to understand the mechanism of enhanced ORR activity.

ARTICLE INFO

Article history:
Received 24 April 2014
Received in revised form
19 May 2014
Accepted 20 May 2014
Available online 7 June 2014

Keywords:
Platinum–copper nanowire
Core–shell nanostructure
Oxygen reduction reaction
Fuel cell catalyst

ABSTRACT

Pt-based core–shell electrocatalysts with one-dimensional (1D) nanostructure show a great opportunity to improve the catalytic activity and durability of pure Pt catalyst for oxygen reduction reaction (ORR). Here, we synthesize Cu@CuPt core@shell nanowires (NWs) with 1D nanostructure by using Cu NWs as templates in organic solvent medium. The ORR mass activity and specific activity of PtCu NWs are 0.216 A mg_{pt}^{-1} and 0.404 mA cm^{-2} at 0.9 V, respectively, which are 3.1 and 3.7 times larger than that of the commercial Pt/C catalyst (0.07 A mg_{pt}^{-1} and 0.110 mA cm^{-2}, respectively). Theoretical studies suggest that the electronic effect of the Cu substrate on the Pt monolayer could be the main reason for the higher activity of PtCu NWs than that of the commercial Pt/C catalyst. In addition, the PtCu NWs show much better durability than the commercial Pt/C catalyst after stability test. It is expected that the as-synthesized PtCu NWs in organic solvent medium could be excellent candidates as high performance catalysts for ORR.

1. Introduction

Proton exchange membrane fuel cells (PEMFCs) are considered to be a promising energy conversion device for the future energy application [1,2]. As is well known, the platinum materials have been regarded as the most effective cathode electrocatalysts for the oxygen reduction reaction (ORR) in PEMFCs [3,4]. However, the high cost, the kinetic limitation of ORR at the cathode, and the durability issues are the main barriers for the commercial applications of pure Pt catalysts [5–7]. Therefore, most investigations have focused on Pt-based bimetallic catalysts such as core–shell nanomaterials or alloying Pt with less expensive early transition metals [8–10], including Fe [11,12], Co [13,14], Ni [15,16], and Cu [17,18], in order to develop more active and durable catalysts that are superior to the commercial carbon-supported platinum (Pt/C) catalyst. Clearly, when a thin shell of Pt or Pt alloy is deposited on the non-Pt core as a Pt-based core–shell structure, both its activity and durability are greatly enhanced [19–21]. In addition, when Pt-based catalysts are prepared in one-dimensional (1D) nanostructure with a controlled shape and a high platinum surface area, they can be highly efficient electrocatalyst for the ORR [22,23]. Moreover, these catalysts with 1D nanostructure would demonstrate better durability than the commercial Pt/C catalyst due to the large surface contact and strong adherence between these products and carbon support [22–24].

In general, Pt-based core–shell electrocatalysts with 1D nanostructure are synthesized by using inexpensive templates, and the size and morphology of the final product can be mainly determined by using templates with different sizes and shapes [25,26]. Cu has been regarded as an important template to synthesize Pt-based core–shell electrocatalysts with 1D nanostructure, due to its low

* Corresponding authors.
E-mail addresses: chengdj@mail.buct.edu.cn (D. Cheng), zhujq@mail.buct.edu.cn (J. Zhu).

http://dx.doi.org/10.1016/j.jpowsour.2014.05.104
0378-7753/

cost and facile synthesis [27,28]. In previous work, Lei et al. [29] synthesized 1D PtCu nanotubes consisting of a PtCu alloy bulk and a Pt-enriched surface by using Cu nanowires (NWs) as templates in an aqueous solution. Moreover, Yan et al. [28] prepared Pt coated Cu NWs with the size of approximately 100 nm by using an aqueous method. More interestingly, the Cu NWs can also be synthesized in an organic media with high size selectivity [30], making them promising as templates to synthesize Pt-based core–shell electrocatalysts with 1D nanostructure. However, to the best of our knowledge, the synthesis of PtCu NWs in an organic media is still lacking.

In this work, we report a nonaqueous method for the synthesis of PtCu NWs by using Cu NWs as templates in organic solvent medium. We examine the electrocatalytic activity and durability of the as-synthesized Cu@CuPt core@shell NWs with 1D nanostructure. When compared with that of the commercial Pt/C catalyst, the PtCu NWs display substantial ORR activity. It is found that the ORR mass activity and specific activity of PtCu NWs are 3.1 and 3.7 times larger than that of the commercial Pt/C catalyst, respectively, which is explained by theoretical calculations. In addition, the durability of the PtCu NWs is significantly superior to that of the commercial Pt/C catalyst. Our results show that the as-synthesized PtCu NWs in organic solvent medium could be excellent candidates as high performance catalysts for ORR.

2. Experimental section

2.1. Synthesis

2.1.1. Chemicals

Cupric (II) acetylacetonate ($Cu(acac)_2$), oleylamine, 1-octadecene, nickel chloride hexahydrate ($NiCl_2{\cdot}6H_2O$), and dimethyl distearylammonium chloride (D1821) were purchased from Aladdin. Platinum (II) acetylacetonate ($Pt(acac)_2$) was purchased from J&K Chemical. Commercial platinum/carbon catalyst (Hispec 3000, 20% Pt/C) was received from Johnson Matthey. Carbon black (Vulcan XC-72R) was obtained from Cabot Company. 5 wt.% Nafion solution was obtained from DuPont Company. All chemicals were used without further purification.

2.1.2. Synthesis of Cu NWs

Cu NWs were achieved by a reduction of $Cu(acac)_2$ with the presence of $NiCl_2{\cdot}6H_2O$ and D1821 in oleylamine medium. Briefly, 0.4 mmol $Cu(acac)_2$, 0.2 mmol $NiCl_2{\cdot}6H_2O$, and 0.25 mmol D1821 were dissolved in 8 ml of oleylamine in a 25 ml three-neck round-bottle flask and kept at 100 °C for 20 min with a strong agitation under a nitrogen (N_2) stream. The flask was then heated to 185 °C for several minutes and sustained for 3 h. Vigorous stirring was maintained throughout all the syntheses. After cooling to the room temperature, the Cu NWs were achieved by centrifugation after adding sufficient hexane at 10,000 rpm for 10 min and repeated this procedure more than three times. The product was dried in N_2 atmosphere to protect the Cu NWs from oxidation afterward.

2.1.3. Synthesis of PtCu NWs

A typical procedure for synthesizing PtCu NWs is as follows: 0.15 mmol Cu NWs was dissolved in 10 ml of 1-octadecene, and then dispersed by ultrasonic irradiation for more than 10 min. Subsequently, they were added into a 25 ml three-neck flask and heated to 205 °C under a N_2 stream. A $Pt(acac)_2$ solution (0.02 mmol $Pt(acac)_2$ dissolved in 10 ml 1-octadecene) was added into the vigorously stirred solution for 10 min and the temperature was kept at 205 °C for 3 h. The resultant product was isolated by centrifugation after adding a sufficient amount of hexane and acetone, and then repeated this procedure for several times. Subsequently, the product was suspended in 10 ml acetic acid for 2 h at room temperature. The final product was separated from the acid by centrifugation and washed with ethanol for several times, and dried at 60 °C overnight.

2.2. Characterization

Powder X-ray diffraction (PXRD) patterns were recorded using Bruker D8 Advance X-ray diffractometer with Cu Ka ($\lambda = 0.15418$ nm) radiation source at 40 kV, 40 mA. Transmission electron microscopy (TEM) images were collected on Tecnai G^2 20 operating at 200 kV. The scanning electron microscope (SEM) images and energy dispersive X-ray spectroscopy (EDX) data were obtained from a Hitachi S-4800 SEM operated at 20 kV. High-Resolution TEM (HRTEM) images were collected on a JEOL JEM-2100 transmission electron microscope. EDX line-scan analysis was recorded on JEOL JEM-2010f with a high-angle annular dark-field scanning TEM (HAADF-STEM). X-ray Photoelectron Spectroscopy (XPS) data were taken on a ThermoFisher ESCALAB 250 X-ray photoelectron spectroscopy with a Mg-Ka source. Metal element content was obtained by Inductively Coupled Plasma Atomic Emission Spectrometer (ICP-AES) using Shimadzu IPCPS-7500.

2.3. Catalyst and working electrode preparations

Carbon black (Vulcan XC-72) was used as support for preparing electrocatalysts. In a typical preparation, the as-prepared product was mixed with carbon black at the product-to-carbon-black mass ratio of 1:4 in 10 ml hexane. Subsequently, the mixture was sonicated for 30 min and precipitated out by centrifugation. The carbon support samples were achieved after drying in air overnight.

The procedure of working electrode preparation for PtCu NWs and the commercial Pt/C catalyst is as follows: 10 mg carbon support sample was added into a 5 ml mixture of deionized water, isopropanol and Nafion (5%) at a volume ratio of 4:1:0.05. After ultrasonic irradiation for at least 30 min, 15 μL catalyst ink was deposited on the glassy carbon-rotating disk electrode (GC-RDE) of 5 mm diameter. Actually, all the catalysts on RDE are approximately 30.6 μg cm^{-2}. The electrode was dried at ambient condition and was used as a working electrode for further electrochemical studies.

2.4. Electrochemical measurements

A three-electrode cell was used to do the electrochemical measurements. A platinum wire was used as the counter electrode and saturated calomel electrode (SCE) was used as the reference electrode. The working electrode was a GC-RDE (diameter: 5 mm and area: 0.196 cm^2). All potentials were converted to values with reference to a reversible hydrogen electrode (RHE). The electrolyte was 0.1 M perchloric acid ($HClO_4$) diluted from 70% using ultrapure water. Cyclic voltammograms (CVs) were obtained by scanning the potentials between 0.05 and 1.30 V versus RHE at a scan rate of 50 mV s^{-1} in N_2-saturated 0.1 M $HClO_4$. ORR polarization curves were obtained by scanning the potentials from 1.25 to 0.05 V versus RHE at a scan rate of 10 mV s^{-1} in oxygen-saturated (O_2-saturated) 0.1 M $HClO_4$ with the GC-RDE rotating at 1600 rpm. For ensuring N_2-saturated or O_2-saturated, the 0.1 M $HClO_4$ solution was purged with N_2 or O_2 more than 30 min prior to the electrochemical measurements. In addition, N_2 or O_2 was maintained over the electrolyte during the measurement. The durability of the catalyst was tested by cycling the potentials between 0.5 and 1.0 V versus RHE at a sweep rate of 50 mV s^{-1} in O_2-saturated 0.1 M $HClO_4$.

The electrochemically active surface area (ECSA) of the catalyst can be estimated by measuring the area of desorption of atomic

hydrogen between 0.05 and 0.40 V versus RHE on the curve of the cyclic voltammograms. The ECSA was calculated based on the following relation:

$$\mathrm{ECSA} = Q_H/(m \times q_H) \quad (1)$$

where Q_H is the charge for hydrogen desorption, m is the loading amount of metal in the electrode, and q_H is the charge required for monolayer desorption of hydrogen on Pt (210 μC cm^{-2}).

For the ORR at a RDE, the Koutecky–Levich equation can be described by the following relation:

$$1/i = 1/i_k + 1/i_d \quad (2)$$

where i is the experimentally measured current, i_k and i_d are the kinetic and diffusion-limited current densities, respectively. Then, the kinetic current was calculated based on the following equation:

$$i_k = (i_d \times i)/(i_d - i) \quad (3)$$

For each catalyst, the kinetic current was normalized to ECSA and the loading amount of metal in order to obtain the specific activity and mass activity, respectively.

2.5. Density-functional theory (DFT) calculations

DFT calculations were performed by using the Vienna Ab-initio Simulation Package (VASP) [31–34]. The generalized gradient approximation GGA of Perdew, Burke, and Ernzerhof (PBE) was used to describe the exchange and correlation potential [35]. The cutoff energy for the plane-wave basis set was set to 430 eV in all calculations. The Monkhorst–Pack mesh k-points ($11 \times 11 \times 11$) and ($5 \times 5 \times 1$) were used for the bulk and slab calculations, respectively. The convergence criteria for the electronic self-consistent iteration and the ionic relaxation loop were set to 10^{-4} eV and 0.05 eV $Å^{-1}$, respectively. We employed the surface models to simulate the PtCu NWs studied in our experiments, wherein the Pt monolayer is placed on the top of the Cu(111) surface, namely the PtCu(111) surface. The binding energy of atomic oxygen on the PtCu(111) and pure Pt(111) surfaces was calculated, which was considered as an effective descriptor for the catalytic activity toward the ORR in our work [36,37]. In DFT calculations, the slab alloys were modeled with a four-layer slab using a 2×2 supercell. A vacuum gap of about 12 Å in the z-direction was introduced to separate two subsequent slabs. The atoms in the top two layers were allowed to relax, while the atoms on the remaining two layers were fixed at their ideal bulk positions. All adsorbates were placed on one side of the slab. The adsorption energies of O at different adsorption sites are defined by

$$E_{\mathrm{ads}} = E_{\mathrm{adsorbate+surface}} - E_{\mathrm{adsorbate}} - E_{\mathrm{surface}} \quad (4)$$

where $E_{\mathrm{adsorbate+surface}}$ is the energy of species adsorption on the surface, E_{surface} is the energy of the clean surface, and $E_{\mathrm{adsorbate}}$ is the energy of the isolated molecule.

3. Results and discussion

3.1. Synthesis and characterization of Cu NWs

Cu NWs were synthesized by a reduction of $Cu(acac)_2$ with the presence of $NiCl_2 \cdot 6H_2O$ and D1821 in oleylamine medium at 185 °C (see Experimental section for details). Oleylamine was used as not only the reducing agents but also a solvent. In addition, oleylamine and D1821 were used as capping agent to control the morphology of NWs in growth.

XRD measurement was carried out to examine the composition of as-prepared production. As shown in Fig. 1A, the peaks at around 43.4°, 50.4°, and 74.3° correspond to the Cu (111), (200) and (220) diffraction ones, respectively. No diffraction peaks of Ni or Cu_2O impurities were observed, indicating that the as-synthesized Cu samples are of high purity and crystallinity. In addition, the absence of Ni or O in Cu sample had also been examined by the analysis of the EDX results. Clearly, there is no characteristic signal belonging to Ni or O in the EDX spectra recorded from these Cu NWs (Fig. 1B). It is noted that the role of Ni in the reaction and formation mechanism of Cu NWs had been discussed in previous work [30].

The SEM and TEM images of as-prepared Cu NWs are shown in Fig. 1C and E. The average diameter of the Cu NWs has been calculated to be 24.6 nm (Fig. 1D) on the basis of 60 individual nanowires in low magnification image (see Fig. S1 in Supplementary material). It is found that the as-synthesized Cu NWs are smaller than these synthesized in aqueous solvent [28], indicating that they are more promising templates to synthesize Pt-based electrocatalysts. The microstructure of Cu NWs was further characterized by using high resolution (HR) TEM. The HRTEM image of Cu NWs in Fig. 1F reveals that the lattice fringe is in the range from 0.205 to 0.209 nm, corresponding to the (111) planes of fcc Cu.

3.2. Synthesis and characterization of PtCu NWs

PtCu NWs were prepared by adding $Pt(acac)_2$ solution into Cu NWs template in 1-octadecene medium at 205 °C (see Experimental section for details). It is found that the ratio between Pt and Cu is directly proportional to that of adding Cu NWs and $Pt(acac)_2$. In addition, the acid treatment can remove the surfactant coating and activate PtCu NWs catalysts.

The morphologies of PtCu NWs were characterized by SEM and TEM, as shown in Fig. 2. It is found that the as-prepared PtCu NWs show a rough surface, which is different from that of Cu NWs. Additionally, the average diameter of the PtCu NWs is calculated to be 36.1 nm, which is much larger than that of pure Cu NWs (24.6 nm), due to the deposition of Pt on the surface of the Cu NWs. Moreover, the HRTEM image of PtCu NWs in the inset of Fig. 2B reveals that the lattice fringe is in the range from 0.216 to 0.220 nm, corresponding to the (111) interplanar distance of fcc PtCu structure.

The elemental compositions of PtCu NWs were characterized by SEM associated with EDX and ICP-AES. From the EDX result (see Fig. S2 in Supplementary material), the Pt loading weight of PtCu NWs is determined to be 27.93%. The overall weight percentage of Pt in the PtCu NWs being measured by ICP-AES is 26.15%, which is consistent with the EDX result. We also performed EDX line-scan analysis to forecast the structure of PtCu NWs, as shown in Fig. 2D. The result collected from an individual nanowire (Fig. 2C) clearly shows that Pt exists at edge while Cu mainly concentrates in the center, indicating that the PtCu NWs is formed by PtCu alloy shell and Cu core.

Information on surface chemistry of the PtCu NWs was investigated by XPS (see Fig. S3 in Supplementary material). The Pt weight of surface of PtCu NWs has been calculated to be 70.30%, which is evidently higher than that of overall PtCu NWs (26.15%). It certifies again that Pt is enriched at the edge of the PtCu NWs. The high and low doublets in the XPS spectroscopy correspond to metallic and oxidized Pt, respectively. It is also found that the Pt4f signal of PtCu NWs shifts to lower binding energy compared to that of the commercial Pt/C catalyst, due to the electron transfer from Cu to Pt. It is noted that such an electron transfer and the compressive surface strain (Cu core) on Pt would downshift the d-band center of Pt, which is beneficial to the catalytic activity and durability [29,38,39].

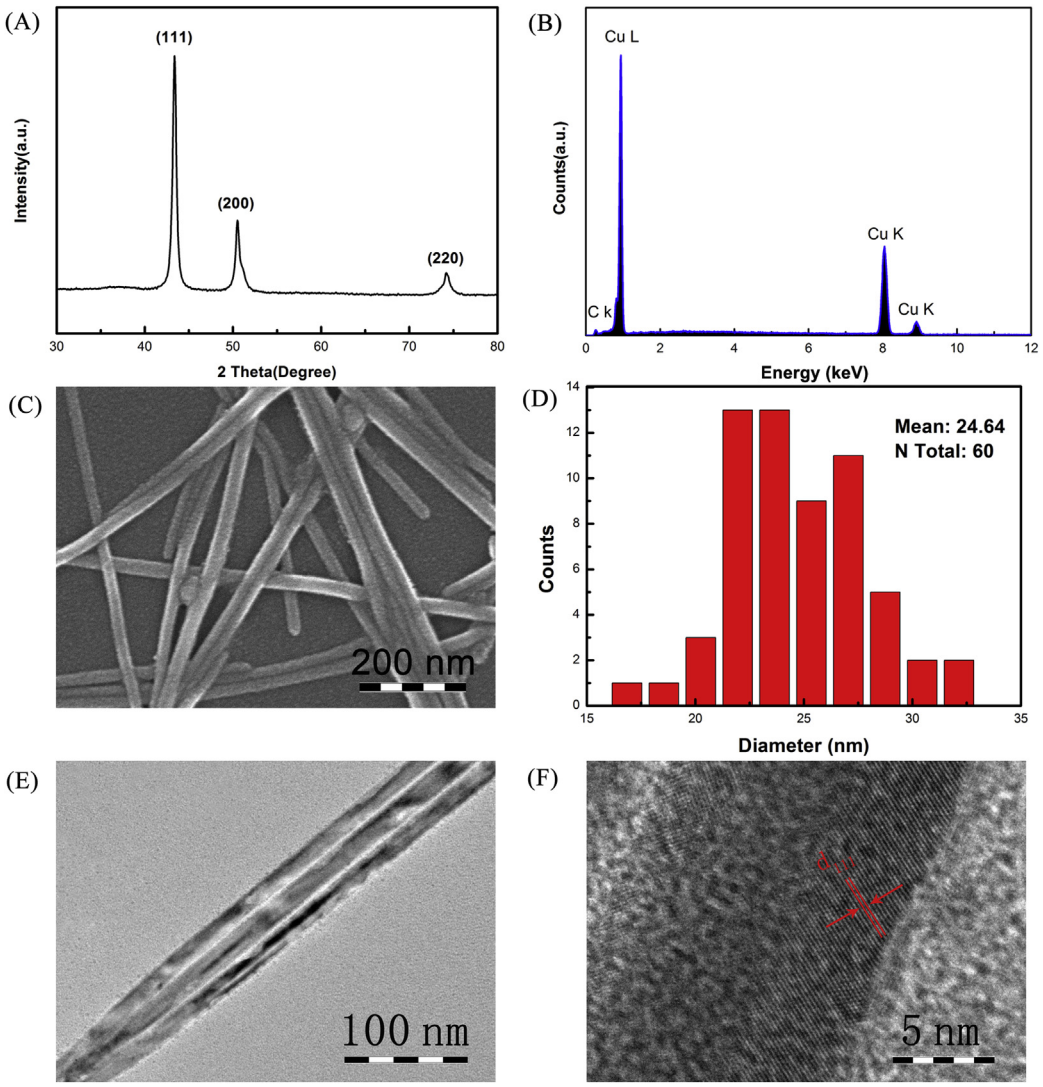

Fig. 1. (A) XRD pattern, (B) EDX spectrum, (C) SEM image, (D) diameter distribution image, (E) TEM image and (F) HRTEM image of Cu NWs.

3.3. Electrochemical properties

Fig. 3A shows the cyclic voltammetry (CV) curves of PtCu NWs and the commercial Pt/C catalyst, recorded at a sweep rate of 50 mV s^{-1} in N_2-purged 0.1 M $HClO_4$ solutions at room temperature (25 °C). In order to obtain steady CV results, the working electrode was cleaned by scanning CV with more than 30 cycles from 0.05 to 1.30 V in N_2-saturated electrolyte. The CV curves exhibit three distinctive potential regions associated with the hydrogen adsorption/desorption processes ($H + e^- = H_{upd}$) in the range from 0.05 to 0.40 V, double layer region from 0.40 to 0.60 V and reversible adsorption of OH_{ad} ($2H_2O = OH_{ad} + H_3O^+ + e^-$) beyond 0.6 V, where H_{upd} and OH_{ad} refer to the under-potentially deposited hydrogen and the adsorbed oxygenated species, respectively. The electrochemically active surface area (ECSA) has been obtained by measuring the hydrogen desorption area. In the calculation, the area is acquired by integration and the electric charge is assumed to be 210 μC cm^{-2} after double-layer correction (see Experimental section for details) [40]. The specific ECSA (the ECSA per unit weight of metal) of the PtCu NWs and the commercial Pt/C catalyst are determined to be 13.99 and 64.27 $m^2\ g^{-1}$, respectively. Based on the Pt mass, the ECSA of the PtCu NWs and the commercial Pt/C catalyst are calculated to be 53.50 and 64.27 $m^2\ g^{-1}$, respectively. It means that PtCu NWs provide a relatively high ECSA, due to the full utilization of Pt on the surface.

The ORR measurements were performed in an O_2-saturated 0.1 M $HClO_4$ solutions by using a glassy carbon rotating disk electrode (RDE) with a sweep of 10 mV s^{-1} and a rotation rate of 1600 rpm at room temperature (25 °C). Actually, all the catalysts on RDE are approximately 30.6 μg cm^{-2} (see Experimental section for details). Fig. 3B shows the ORR polarization curves for PtCu NWs and the commercial Pt/C catalyst at the same conditions. For all of these catalysts, the diffusion-limiting current region ranges from 0.05 to 0.6 V versus RHE, whereas a mixed kinetic-diffusion control region occurs between 0.6 and 1.0 V versus RHE. The ORR half-wave potential ($E_{1/2}$) of the commercial Pt/C catalyst (0.869 V versus RHE) is more positive than that of PtCu NWs (0.853 V versus RHE). In addition, the value of $E_{1/2}$ can be greatly affected by the total Pt loading weight. In order to compare the activities of different catalysts, the catalytic activities are also evaluated by mass activity and specific activity, which are obtained by normalizing the kinetic current to loading mass and the ECSA of Pt, respectively. Fig. 3C shows the mass activity and specific activity of PtCu NWs and the commercial Pt/C catalyst. It is found in Fig. 3C that the PtCu NWs

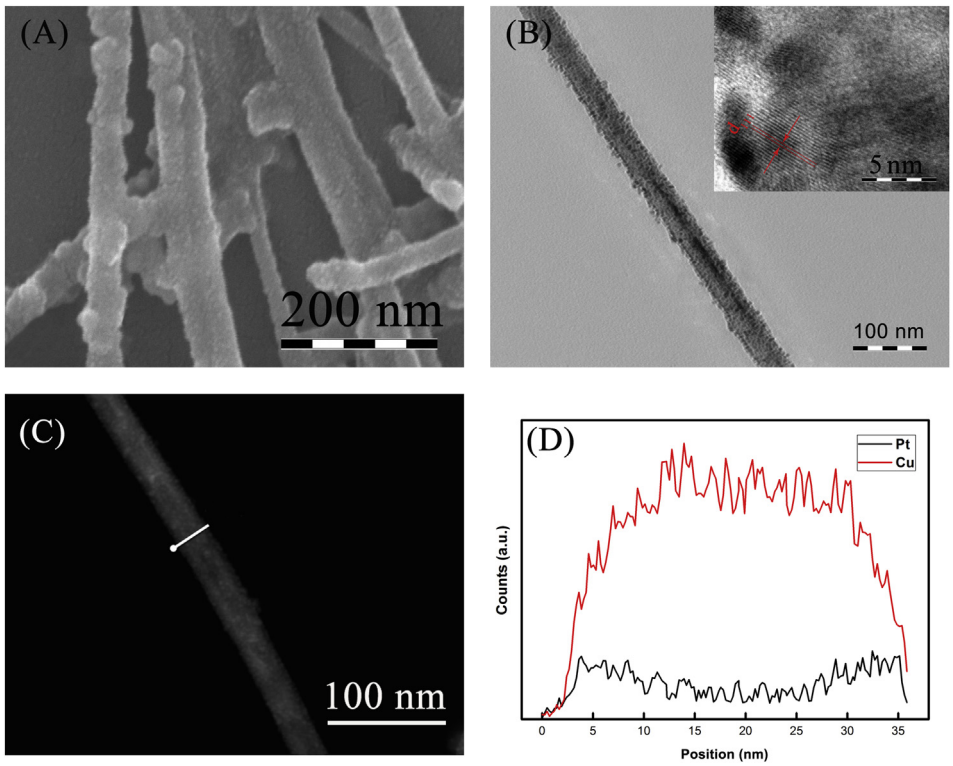

Fig. 2. (A) SEM image, (B) TEM image, (C) HADDF-STEM image and (D) corresponding EDX line profiles of PtCu NWs. The inset in (B) is HRTEM of PtCu NWs.

exhibit the mass activity of 0.216 A mg_{pt}^{-1} on the basis of the Pt mass at 0.9 V versus RHE, which is 3.1 times larger than that of the commercial Pt/C catalyst (0.109 A mg_{pt}^{-1}). In addition, as shown in Fig. 3C, the specific activity of PtCu NWs is 0.404 mA cm^{-2}, which is 3.7 times larger than that of the commercial Pt/C catalyst (0.110 mA cm^{-2}). Our results show that PtCu NWs served as electrocatalysts for ORR are much superior to the commercial Pt/C catalyst.

Recent investigations [26,28,41] have revealed that the high utilization of Pt atoms on the surface of a catalyst would enhance the activity. In general, when most of the Pt atoms were deposited on the surface, they would be directly involved in ORR, which can greatly increase the mass activity. In this work, the PtCu NWs were prepared by depositing Pt with a controlling thickness on Cu NWs, which can improve the ORR activity by enhancing the Pt utilization and mass transport in electrolyte. The PtCu NWs with 1D structure also can facilitate the diffusion of O_2 on the surface of the catalyst compared to the 0D commercial Pt/C catalyst [6].

DFT calculations are used to understand the mechanism of enhanced ORR activity, and the models of the PtCu(111) and pure Pt(111) surfaces are shown in Fig. 3D. In our calculations, the interaction of the Pt-monolayer with the Cu support can cause a reconstruction of electronic structure of surface Pt atoms, when compared with the Pt atoms in the top layer of the Pt(111) surface. It is found that there is a downshift in the d-band center of surface Pt atoms, as shown in Fig. 3D. The downshift of d-band center could dramatically enhance the catalyst activity for ORR that have confirmed by previous research [24,42]. Table S1 lists all the adsorption energies of oxygen atom on these surfaces at different adsorption sites. As shown in Fig. 3D, the downshift in d-band center position is justly reflected in changes in the adsorption energies of oxygenated intermediates at the most favorable adsorption site. It suggests that a single metric, which captures the relationship between the electronic properties of metallic surfaces and the adsorption energies of oxygenated intermediates, is the d-band center [43]. Our results show that the formation of a Pt monolayer in the Cu(111) can shift the d-band center far from the Fermi level and result in a reduced adsorption strength of O, benefiting the exposure of catalyst activity sites and facilitating oxygenated intermediates adsorption and desorption, thereby increasing the ORR activity greatly.

The durability of PtCu NWs and the commercial Pt/C catalyst was tested by cycling the potential between 0.5 and 1.0 V versus RHE at a sweep rate of 50 mV s^{-1} in O_2-saturated 0.1 M $HClO_4$. The cyclic voltammetry and polarization curves for PtCu NWs and the commercial Pt/C catalyst before and after 10,000 cycles are shown in Fig. 4. It is found that, after 10,000 cycles, 80.5% and 61.6% of the original ECSA are maintained for PtCu NWs and the commercial Pt/C catalyst, respectively. In addition, the $E_{1/2}$ shift of PtCu is smaller than that of the commercial Pt/C catalyst. It means that the PtCu NWs show much better durability than the commercial Pt/C catalyst.

In order to investigate the decreasing tendency of ECSA for these catalysts, the ECSA was recorded at different cycling numbers. The normalized ECSA in terms of cycling numbers for PtCu NWs and the commercial Pt/C catalyst is shown in Fig. 5A. Evidently, PtCu NWs exhibit much slower decreasing tendency compared with the commercial Pt/C catalyst. Moreover, the mass activity and specific activity of these catalysts before and after 10,000 cycles are calculated and shown in Fig. 5B and C, respectively. The mass activity loss for PtCu NWs is only 16.5% after 10,000 cycles, which is less than that of the commercial Pt/C catalyst (43.0%). In addition, the PtCu NWs has a mass activity of 0.180 A mg_{pt}^{-1} and specific activity of 0.419 mA cm^{-2} after 10,000 cycles, which are 4.5 and 4.1 times larger than that of the commercial Pt/C catalyst (0.040 A mg_{pt}^{-1} and 0.102 mA cm^{-2}, respectively). As is well known, the durability issue of electrocatalyst can be attributed to the loss of ECSA, which is associated with the corrosion of carbon support, the dissolution of

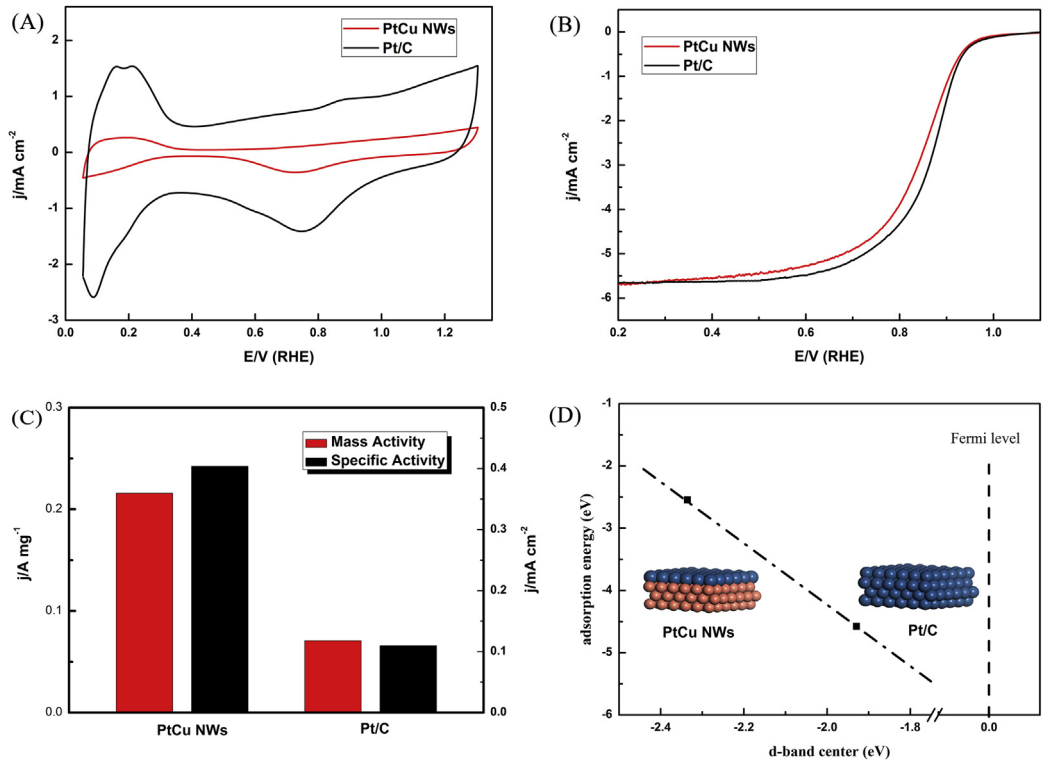

Fig. 3. Comparison of electrocatalytic properties of PtCu NWs and the commercial Pt/C catalyst. (A) CVs of PtCu NWs, and the commercial Pt/C catalyst recorded in N_2-saturated 0.1 M $HClO_4$ at a scan rate of 50 mV s^{-1}. (B) ORR polarization curves for PtCu NWs and the commercial Pt/C catalyst recorded in O_2-saturated 0.1 M $HClO_4$ at a scan rate of 10 mV s^{-1} and a rotation rate of 1600 rpm. (C) ORR mass activity and specific activity for PtCu NWs and commercial Pt/C catalyst at 0.9 V versus RHE. (D) Models and the d-band center of top-layer atoms versus the adsorption energy of atomic oxygen at the most favorable adsorption site for the Pt(111) and PtCu(111) surfaces.

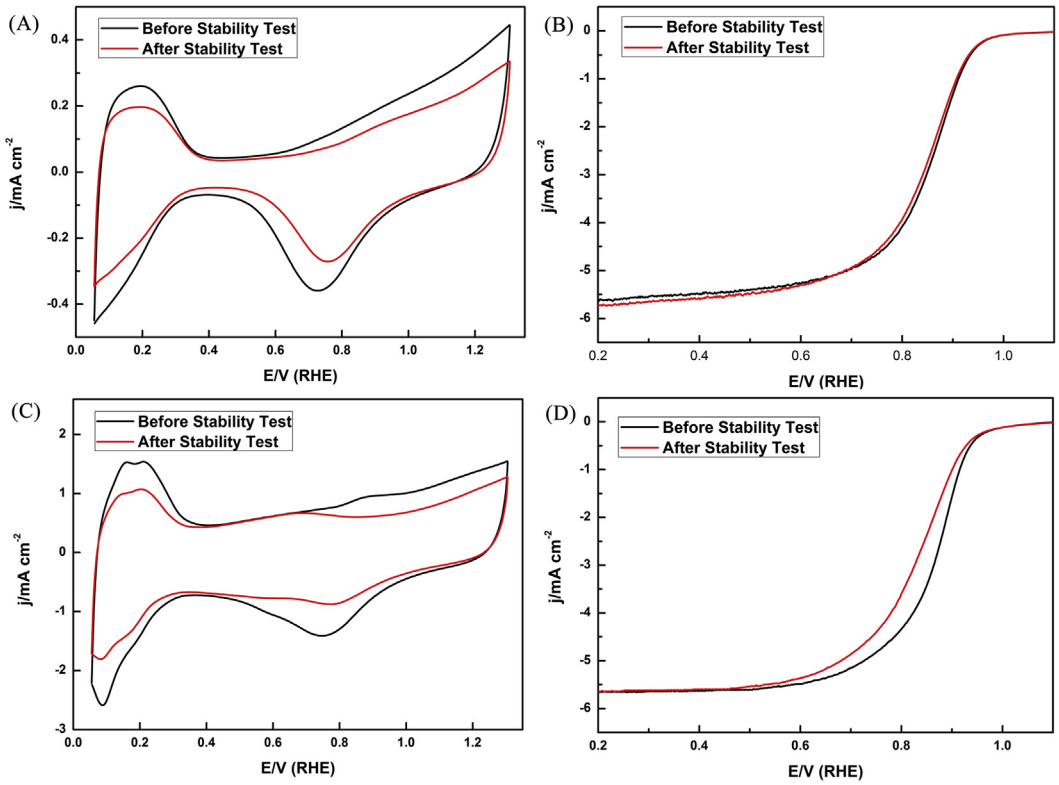

Fig. 4. CVs of PtCu NWs (A) and the commercial Pt/C catalyst (C) before and after stability test. ORR polarization curves of PtCu NWs (B) and the commercial Pt/C catalyst (D) before and after stability test. The stability test was tested by cycling the potential between 0.5 and 1.0 V versus RHE in O_2-saturated 0.1 M $HClO_4$ at a sweep rate of 50 mV s^{-1} for 10,000 cycles.

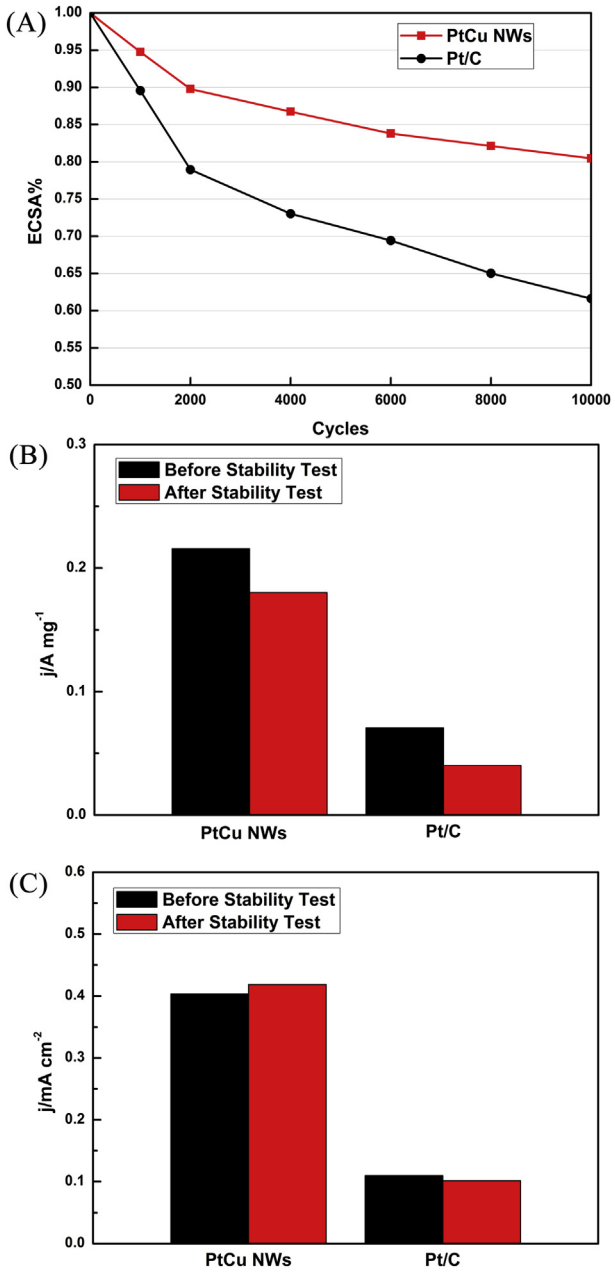

Fig. 5. (A) ECSA change of PtCu NWs and the commercial Pt/C catalyst as a function of cycles during stability test. ORR mass activity (B) and specific activity (C) for PtCu NWs and the commercial Pt/C catalyst at 0.9 V before and after stability test.

Pt and the aggregation of Pt nanoparticle [44,45]. In this work, PtCu NWs with micrometer scale length can strengthen the adherence with carbon black and decrease the aggregation and dissolution of Pt, thereby decreasing the loss of ECSA and enhancing durability.

4. Conclusions

In summary, a nonaqueous method was explored to synthesize Cu@CuPt core@shell nanowires (NWs) with one-dimensional (1D) nanostructure by using Cu NWs as templates in organic solvent medium. The electrochemical measurements reveal that the as-synthesized PtCu NWs exhibit mass activity and specific activity of 0.216 A mg_{pt}^{-1} and 0.404 mA cm^{-2} at 0.9 V, which are 3.1 and 3.7 times larger than that of the commercial Pt/C catalyst. Our theoretical studies suggest that the higher activity of PtCu NWs than the commercial Pt/C catalyst could be mainly caused by the electronic effect of the Cu substrate on the Pt monolayer. In addition, the PtCu NWs maintain higher relative ECSA and ORR activity compared with the commercial Pt/C catalyst after stability test. Our results show that the as-synthesized PtCu NWs in organic solvent medium can improve the activity and stability of the commercial Pt/C catalyst, which could potentially be used as high performance electrocatalysts for ORR.

Acknowledgments

This work is supported by the National Natural Science Foundation of China (21106003, 21176010, 91334203), Beijing Higher Education Young Elite Teacher Project and Beijing Novel Program (Z121110000250000).

Appendix A. Supplementary data

Supplementary data related to this article can be found at http://dx.doi.org/10.1016/j.jpowsour.2014.05.104.

References

[1] B.C. Steele, A. Heinzel, Nature 414 (2001) 345–352.
[2] R. Borup, J. Meyers, B. Pivovar, Y.S. Kim, R. Mukundan, N. Garland, D. Myers, M. Wilson, F. Garzon, D. Wood, Chem. Rev. 107 (2007) 3904–3951.
[3] M.L. Perry, T.F. Fuller, J. Electrochem. Soc. 149 (2002) S59–S67.
[4] M. Winter, R.J. Brodd, Chem. Rev. 104 (2004) 4245–4270.
[5] B. Lim, M. Jiang, P.H. Camargo, E.C. Cho, J. Tao, X. Lu, Y. Zhu, Y. Xia, Science 324 (2009) 1302–1305.
[6] Y. Qiao, C.M. Li, J. Mater. Chem. 21 (2011) 4027–4036.
[7] J. Wu, H. Yang, Acc. Chem. Res. 46 (2013) 1848–1857.
[8] H.A. Gasteiger, S.S. Kocha, B. Sompalli, F.T. Wagner, Appl. Catal. B 56 (2005) 9–35.
[9] N. Travitsky, T. Ripenbein, D. Golodnitsky, Y. Rosenberg, L. Burshtein, E. Peled, J. Power Sources 161 (2006) 782–789.
[10] S. Guo, S. Zhang, S. Sun, Angew. Chem. Int. Ed. Engl. 52 (2013) 8526–8544.
[11] W. Chen, J. Kim, S. Sun, S. Chen, J. Phys. Chem. C 112 (2008) 3891–3898.
[12] S. Guo, D. Li, H. Zhu, S. Zhang, N.M. Markovic, V.R. Stamenkovic, S. Sun, Angew. Chem. Int. Ed. 52 (2013) 3465–3468.
[13] E. Antolini, J. Salgado, M. Giz, E. Gonzalez, Int. J. Hydrogen Energy 30 (2005) 1213–1220.
[14] P. Yu, M. Pemberton, P. Plasse, J. Power Sources 144 (2005) 11–20.
[15] H.R. Colón-Mercado, H. Kim, B.N. Popov, Electrochem. Commun. 6 (2004) 795–799.
[16] S.J. Bae, S.J. Yoo, Y. Lim, S. Kim, Y. Lim, J. Choi, K.S. Nahm, S.J. Hwang, T.-H. Lim, S.-K. Kim, J. Mater. Chem. 22 (2012) 8820–8825.
[17] G. Gupta, D.A. Slanac, P. Kumar, J.D. Wiggins-Camacho, X. Wang, S. Swinnea, K.L. More, S. Dai, K.J. Stevenson, K.P. Johnston, Chem. Mater. 21 (2009) 4515–4526.
[18] K. Neyerlin, R. Srivastava, C. Yu, P. Strasser, J. Power Sources 186 (2009) 261–267.
[19] V. Mazumder, M. Chi, K.L. More, S. Sun, J. Am. Chem. Soc. 132 (2010) 7848–7849.
[20] A. Sarkar, A. Manthiram, J. Phys. Chem. C 114 (2010) 4725–4732.
[21] H.H. Li, C.H. Cui, S. Zhao, H.B. Yao, M.R. Gao, F.J. Fan, S.H. Yu, Adv. Energy Mater. 2 (2012) 1182–1187.
[22] H. Zhou, W.-p. Zhou, R.R. Adzic, S.S. Wong, J. Phys. Chem. C 113 (2009) 5460–5466.
[23] H. Zhu, S. Zhang, S. Guo, D. Su, S. Sun, J. Am. Chem. Soc. 135 (2013) 7130–7133.
[24] S. Guo, S. Zhang, D. Su, S. Sun, J. Am. Chem. Soc. 135 (2013) 13879–13884.
[25] Z. Peng, H. Yang, Nano Today 4 (2009) 143–164.
[26] H. Zhang, M. Jin, J. Wang, W. Li, P.H. Camargo, M.J. Kim, D. Yang, Z. Xie, Y. Xia, J. Am. Chem. Soc. 133 (2011) 6078–6089.
[27] M. Mohl, D. Dobo, A. Kukovecz, Z. Konya, K. Kordas, J. Wei, R. Vajtai, P.M. Ajayan, J. Phys. Chem. C 115 (2011) 9403–9409.
[28] S.M. Alia, K. Jensen, C. Contreras, F. Garzon, B. Pivovar, Y. Yan, ACS Catal. 3 (2013) 358–362.
[29] L. Su, S. Shrestha, Z. Zhang, W. Mustain, Y. Lei, J. Mater. Chem. A 1 (2013) 12293–12301.
[30] H. Guo, Y. Chen, H. Ping, J. Jin, D.L. Peng, Nanoscale 5 (2013) 2394–2402.
[31] G. Kresse, J. Hafner, Phys. Rev. B 47 (1993) 558.
[32] G. Kresse, J. Hafner, Phys. Rev. B 49 (1994) 14251.
[33] G. Kresse, J. Furthmüller, Comput. Mater. Sci. 6 (1996) 15–50.
[34] G. Kresse, J. Furthmüller, Phys. Rev. B 54 (1996) 11169.

[35] J.P. Perdew, K. Burke, M. Ernzerhof, Phys. Rev. Lett. 77 (1996) 3865.
[36] D. Cheng, W. Wang, Nanoscale 4 (2012) 2408–2415.
[37] W. Xu, D. Cheng, M. Niu, X. Shao, W. Wang, Electrochim. Acta 76 (2012) 440–445.
[38] V.R. Stamenkovic, B. Fowler, B.S. Mun, G. Wang, P.N. Ross, C.A. Lucas, N.M. Marković, Science 315 (2007) 493–497.
[39] J. Yang, X. Chen, X. Yang, J.Y. Ying, Energy Environ. Sci. 5 (2012) 8976–8981.
[40] T. Schmidt, H. Gasteiger, G. Stäb, P. Urban, D. Kolb, R. Behm, J. Electrochem. Soc. 145 (1998) 2354–2358.
[41] C. Du, M. Chen, W. Wang, Q. Tan, K. Xiong, G. Yin, J. Power Sources 240 (2013) 630–635.
[42] J. Zhang, Y. Mo, M. Vukmirovic, R. Klie, K. Sasaki, R. Adzic, J. Phys. Chem. B 108 (2004) 10955–10964.
[43] V.R. Stamenkovic, B.S. Mun, K.J. Mayrhofer, P.N. Ross, N.M. Markovic, J. Am. Chem. Soc. 128 (2006) 8813–8819.
[44] Z. Chen, M. Waje, W. Li, Y. Yan, Angew. Chem. Int. Ed. 46 (2007) 4060–4063.
[45] Y. Shao, G. Yin, Y. Gao, J. Power Sources 171 (2007) 558–566.